Experimental Study of DMT Blade in Sand Using Particle Image Velocimetry

Javier Fumeron[1#], *Felipe* Villalobos[1], *Francisco* Acuña[2], and *Ricardo* Moffat[3]

[1]*Universidad Católica de la Santísima Concepción, Alonso de Ribera 2850, Concepción, Chile.*
[2]*Aragón Ingeniería de Suelos Ltda., Concepción, Chile*
[3]*LMMG Geotechnics & Faculty of Engineering and Sciences, Universidad Adolfo Ibáñez, Santiago, Chile*
[#]*Corresponding author: jfumeron@magister.ucsc.cl*

ABSTRACT

In the study of geotechnical problems, numerical methods such as finite and discrete elements are progressively more used, sometimes overlooking experimental studies. Therefore, this work emphasizes the importance of physical experimentation, applying a digital image correlation (DIC) methodology. For this research, particle image velocimetry (PIV) was chosen using the GeoPIV-RG software. A model replicating the geometry of a full-scale DMT blade was used to evaluate its impact. An experimental setup was designed and built to recreate the driving of this geometry in dry and loose Bío-Bío sand, recording the process through photographs for analysis by PIV. Results show cumulative displacements, displacement patterns according to depth, and analysis of incremental shear deformation. A displacement direction analysis was carried out. It is concluded that the displacement pattern generated by its driving corresponds to an angle much smaller than what is reported for the CPT, and the incremental shear strain does not exceed 2% during the driving process.

Keywords: PIV; DMT; sand deformation.

1. Introduction

In-situ testing methods, such as the flat dilatometer (DMT) and the cone penetration test (CPT), involve inserting equipment into the ground that, inevitably, causes a disturbance in its structure. This disturbance, caused by the downward movement of the DMT blade or cone, relocates soil particles, creating an altered zone whose characteristics vary depending on the shape of the instrument used. The present research focuses on determining through experimental methods the degree and nature of the alterations caused by the insertion of the DMT blade into the soil.

The Flat Dilatometer (DMT), developed in the middle of the 1970s by Marchetti (1980), is a standardized tool whose use follows norms such as ASTM D6635 (2015) and Eurocode 7 (2007). This equipment consists of a stainless-steel blade with a membrane that expands through pneumatic pressure. The expansion of the membrane provides crucial readings, such as the lift-off pressure (reading A) and full expansion upon reaching 1.1 mm (reading B), from which geotechnical parameters are estimated. The accuracy of the geotechnical parameters estimated from two basic readings largely depends on the conditions under which these readings are performed. Therefore, it is crucial to ensure that the conditions during the taking of these readings are optimal to guarantee reliable results. In particular, the readings can be affected by the physical conditions of the soil before the lift-off phase, termed 'reading A'. These conditions are significantly influenced by the movement of the blade through the soil.

Soil deformation caused by driving is more pronounced in areas with greater geometric extent or abruptness, intensifying as the process progresses. Although Baligh and Scott (1975) already recognized and estimated this disturbance for specific cases of a cone and a wedge, research in this field continues, employing a variety of advanced techniques. Among the most prominent are numerical methods, including finite element analysis, with relevant studies by Luo and Xu (2012), Bałachowski (2006), and Bertoli (2017), as well as the discrete element method, highlighted in research by Xu and Frost (2015), Frost et al. (2016), and Butlanska et al. (2018).

Experimental methods, such as research conducted in calibration chambers (Bałachowski 2006; Lee et al. 2011), play a crucial role in validating numerical simulations associated with the driving process. These experimental approaches help overcome the inherent limitations of mathematical models and provide a more robust and reliable basis for interpreting the results. This synergy between experimentation and numerical simulation is fundamental for advancement in understanding and accuracy in this field of study.

In this context, the technique of Digital Image Correlation (PIV/DIC) emerges as a non-invasive and effective experimental method for measuring displacement. This technique is based on digital image processing combined with numerical calculation. Various studies have applied PIV/DIC to a wide range of geotechnical problems; notable examples include pile driving (White and Bolton 2002), exploring the deformation mechanism in footings (Stanier and White 2013), investigating the cone penetration test (Mo, Marshall, and Yu 2012; Arshad et al. 2014; Melnikov and

Boldyrev 2014), among others. Given its proven effectiveness in these studies and high level of precision (Nazhat and Airey 2011; Ngo and Kieu-Le 2021), the PIV/DIC method is considered particularly suitable for examining the effects of DMT driving.

In this study, the DIC technique, implemented in the GeoPIV-RG software by Stanier et al. (2016), is employed to examine the displacement field generated during the DMT insertion. To this end, the real-scale driving process is simulated in a test chamber, capturing photographs of the entire procedure for subsequent analysis using DIC. This research focuses on evaluating the data obtained from the displacement field, which are calculated using the PIV method.

2. Materials and methods

2.1. Physical model experimental system

2.1.1. Preliminary small-scale

In the initial phase of the study, a preliminary small-scale setup was carried out to refine crucial aspects of the experiment. This initial stage was essential for adjusting details such as the type of lighting and verifying that the GeoPIV-RG software could capture displacements in Biobío sand (high contrast sand).

This preliminary experimental setup was more basic, using a manual driving system with various lighting configurations. Both conventional AC light sources and battery-powered lights were tested to obtain continuous light and avoid flickering that could affect measurements. In addition, different types of cameras were evaluated, from mobile phone cameras to professional-grade cameras (Nikon Z6).

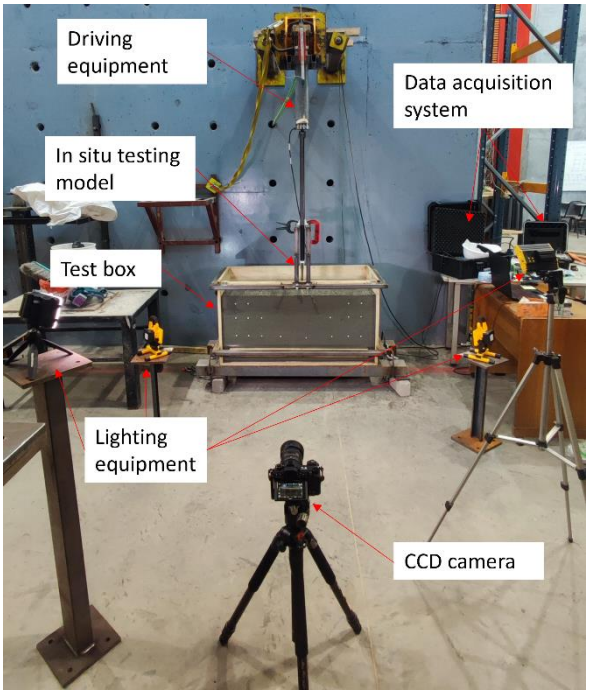

Figure 1. Experimental test equipment

This process allowed for establishing the optimal parameters for the final experimental model, described in detail below.

2.1.2. Final assembly at full scale

The experimental test was carried out in a box equipped with a glass panel, where a sand sample was placed. To simulate the driving process of in-situ exploration devices, real-scale models of the DMT blade were used. This prototype was buried in the sand to replicate the actual driving process. The entire procedure was recorded through the glass panel and documented using photographic sequences.

The experimental model, illustrated in Fig. 1, includes a driving system composed of a linear actuator, a horizontal reaction frame, and instrumentation consisting of a 9000 N load cell with a precision of 0.1 N and a 300 mm Linear Variable Displacement Transducer (LVDT) with a precision of 0.01 mm. In addition, a high-resolution camera and continuous current lighting equipment were used. The test box, made of 21 mm thick structural plywood, with dimensions of 1200 mm in length, 500 mm in width, and 650 mm in height, had a 9 mm thick glass wall. This glass wall was reinforced with two metal stirrups to minimize unwanted displacements during the test.

2.2. Image system

In this study, the Particle Image Velocimetry (PIV) technique was employed to analyse soil deformation during a driving experiment. For image capture, a Nikon Z6 camera with a resolution of 3936 × 2624 pixels was used. To optimize image processing, the image acquisition frequency was set at 5 Hz. The PIV analysis allowed for the observation of soil displacement and deformation fields, including volumetric and shear deformations. The spatial displacement field was determined by comparing and analysing images taken at the beginning of loading and at various instances during the test. For image correspondence before and after deformation, the cross-correlation method in the Fourier domain was applied. Furthermore, surface fitting methods were integrated into sub-pixel positioning approaches to enhance digital image processing. The main title of the article starts with a capital letter followed by lowercase letters with the exemption of names.

White (2003) provides a detailed description of the PIV algorithm used. The shear and volumetric deformation fields were calculated from the differences in the displacement fields, according to the formulas presented in Eq. (1). In these equations, ϵ_x and $\epsilon_y$represent the deformations in the x and y directions, respectively, assuming a positive load direction. γ_{xy} indicates shear strain while ϵ_v represents volumetric deformation, where positive values suggest expansion

$$\left.\begin{aligned}
\epsilon_x &= \frac{\partial u}{\partial x} + \frac{1}{2}\left[\left(\frac{\partial u}{\partial x}\right)^2 + \left(\frac{\partial v}{\partial x}\right)^2\right] \\
\epsilon_y &= \frac{\partial v}{\partial y} + \frac{1}{2}\left[\left(\frac{\partial u}{\partial y}\right)^2 + \left(\frac{\partial v}{\partial y}\right)^2\right] \\
\gamma_{xy} &= \frac{\partial u}{\partial y} + \frac{\partial v}{\partial x} + \left[\frac{\partial u}{\partial x}\frac{\partial u}{\partial y} + \frac{\partial v}{\partial x}\frac{\partial v}{\partial y}\right] \\
\epsilon_v &= \epsilon_x + \epsilon_y
\end{aligned}\right\} \quad (1)$$

and negative values contraction. This approach allowed for a detailed understanding of the soil deformation dynamics under specific load conditions.

While the method developed by White (2003) showed promising results, it required significant refinements. This gap was effectively filled by the Matlab module, GeoPIV-RG, introduced by Stanier et al. (2016). This module significantly improves previous methods, addressing issues of mismatch and random errors inherent in the 'leapfrog' and 'sequential' schemes. Incorporating a Reliability-Guided (RG) approach, initially proposed by Pan et al. (2009) and implemented in Matlab by Blaber et al. (2015), GeoPIV-RG represents a significant advancement over its predecessor, GeoPIV. The key technique of this development is the ability to deform each subset of the reference image through a shape function. This function describes first-order deformations, combined with advanced image intensity interpolation techniques, optimizing the correlation between reference and target subsets (Schreier and Sutton 2002; Stanier et al. 2016). An initial calibration subset, termed the 'seed subset', is analysed so that the RG calculations are based on the optimization parameters obtained in this initial phase. Since the 'seed' is placed in an area with minimal deformations, it offers high and stable correlation values, facilitating the safe optimization of the deformation parameters specified in Eq. (1). Subsequently, the calculations are preconditioned using the results of the most correlated neighbouring subset. Unlike the sequential scheme, the reference image is only updated if the correlation coefficient for the seed or one of the subsets exceeds the user-defined thresholds. This less frequent update is particularly advantageous in sequences with low deformations, as it maintains better correlation and minimizes random errors (Stanier et al. 2016).

2.3. Materials

For this research, Bío-Bío sand was utilized. It is a dark sand with a considerable amount of basalt and quartz, which creates a more significant contrast. The sand was classified as uniform sand (SP) according to the Unified Soil Classification System (USCS) by standard ASTM422 (2017), with uniformity and curvature coefficients of $c_u = 2.55$ and $c_c = 0.84$, respectively. The densities were determined using the methodology proposed in the standard ASTM D4254 (2016), obtaining a maximum of 1.830 g/cm^3 and a minimum of 1.558 g/cm^3. For these densities, the minimum void ratio corresponds to 0.530 (e_{min}) while the maximum is 0.779 (e_{max}), respectively.

It is worth mentioning that the internal friction angle of this sand, specified for a relative density of 38%, was calculated at ϕ=38.7°. Furthermore, the specific gravity of the solids (G_s) was 2.772.

The model of the DMT equipment was crafted using metal and respecting the exact dimensions of the real equipment. However, since the research focuses on the analysis of plane deformations, a symmetric approach is employed by considering only half of the section of the actual equipment.

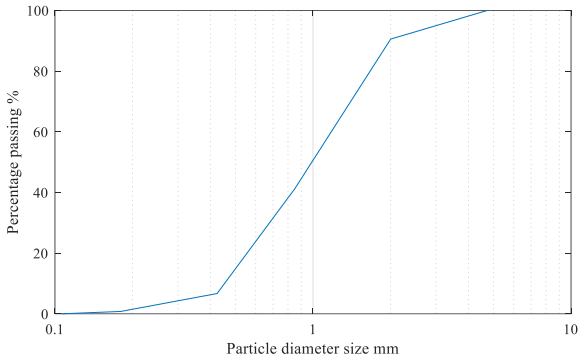

Figure 2. Particle size distribution

2.4. Test scheme

The preparation of the sand sample for the tests follows the ASTM D4254 (2016) standard, specifically designed to determine the relative density. This procedure starts with the continuous deposition of sand in its loosest state, in successive layers, until reaching a height of 50 cm in the test box. Subsequently, the DMT blade is driven from the soil surface, using a linear actuator that ensures a constant speed of 3 mm/s to a depth of 210 mm.

During the driving process, photographs are taken for subsequent analysis using the PIV method. After completing the test, the weight and volume of the sample are measured to verify the achieved density, thus ensuring the reproducibility of the tests, and determining the effective relative density of the sample. In the presented test, relative densities of 16% were achieved. The meticulous filling procedure and subsequent verification of actual density are fundamental to ensure the accuracy and validity of the results obtained in the study's results section.

3. Test results and analysis

The PIV analysis considered a total of 314 photographs. These pictures record the driving of the DMT to a depth of 185 mm, with a difference of 0.58 mm between each picture. The driving process recreated in the glass panel of the experimental montage is illustrated in Fig. 3 for three different instances.

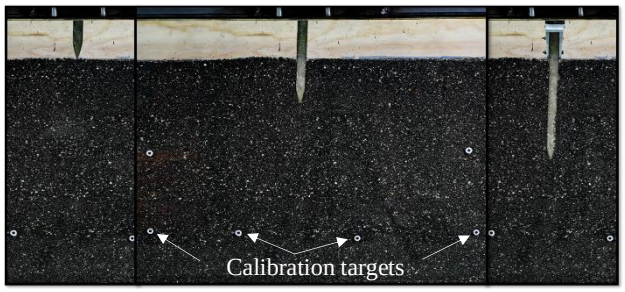

Figure 3. DMT driving process

The results have been sorted into three distinct categories: (1) Cumulative displacements during the insertion process, (2) Displacement patterns during insertion and (3) Deformation levels during driving.

3.1. Accumulated displacement during wedge penetration

The results obtained using GeoPIV-RG were the displacement vectors of each pixel subset, measured in pixels, illustrated in Fig. 4. Subsequently, these vectors were transformed to object space using the calibration targets shown in Fig. 3. This step allowed the conversion of data from the digital space to real space, expressing the measurements in millimetres. Thus, the determination of the displacement surrounding the wedge during the driving process is obtained.

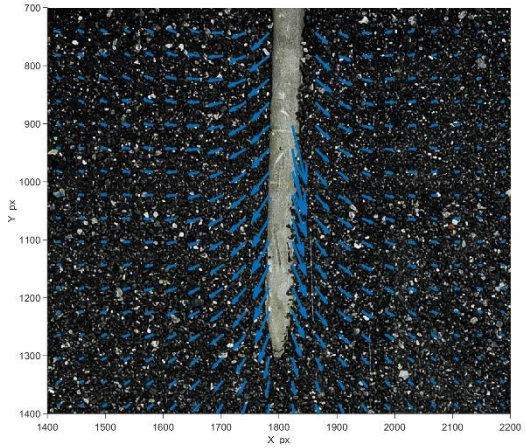

Figure 4. Post-penetration accumulated displacement field vectors in pixels

The analysis results are shown in Fig. 5, where 5(a) illustrates the horizontal displacements, 5(b) the vertical displacements, and 6(c) the contour of the resulting displacement field, integrating the effects of the vertical and horizontal components.

These plots show that the perturbation surrounding the DMT blade has a significant impact. In terms of the horizontal component, this perturbation extends approximately 100 mm to the side of the wedge, with a displacement magnitude of 1.5 mm. On the other hand, the perturbation associated with the vertical component is minor, achieving less than 85 mm from the blade tip, with a displacement magnitude of 1.5 mm. The selection of 1.5 mm was made for easier analysis of the results since in this way the magnitudes of displacement can be adequately covered with the contours shown.

3.2. Soil displacement pattern during wedge penetration

To analyse the displacement pattern during the wedge penetration, the measurements were normalized based on half the thickness of the wedge, with a reference value of r_w = 7.5 mm. This analysis was carried out by selecting a range of 51 photographs, representing a progression of 29.9 mm (equivalent to 3.9 r_w). In Fig. 6, three subfigures are presented corresponding to different initial depths (h), using the h/r_w ratio of normalization. These normalized depths are 7.7, 12.5, and 20 for Figs. 6(a), 6(b), and 6(c), respectively.

In Fig. 6(a), (b), and (c), the displacement vectors resulting from the previously mentioned incremental displacement are highlighted and scaled to facilitate the appreciation of their direction. A segmented red box outlines the section selected for calculating the average displacement direction, shown by the green vector on the wedge right side. Upon performing this calculation, an increase in the displacement vector angle was noted as a deeper starting point was chosen. This led to further

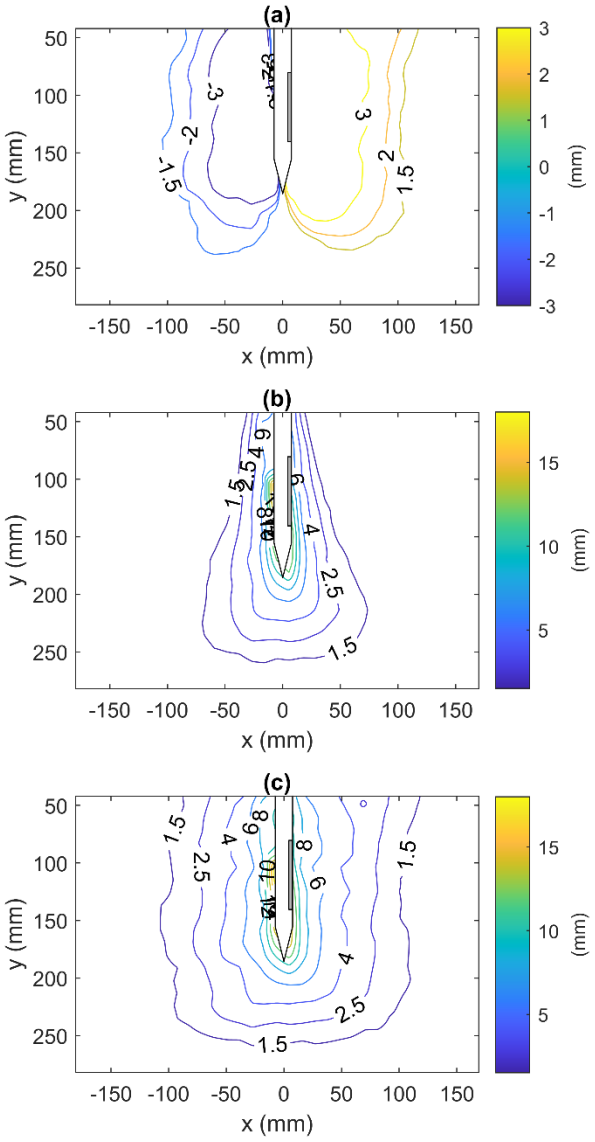

Figure 5. Post-penetration accumulated displacement contours; (a) horizontal component; (b) vertical component; (c) resultant

analysis to determine if this pattern was consistent in other cases. In Fig. 7, this behaviour is illustrated by selecting different starting points (photograph), revealing a trend towards a stable displacement angle, of approximately 21 degrees. In this graphic, the average angle starts on negative values. This occurs because they initially predominate upward vertical displacement

vectors. Therefore, the negative values represent soil heave.

This graphical representation is enlightening, showing how the average direction of the displacement vectors increases with depth. This phenomenon is consistent with patterns observed in pile driving, as reported in previous studies (White and Bolton 2002). Initially, an average displacement direction of 3.7 degrees is observed, which gradually increases to 21 degrees upon completion of the driving process. This change is attributed to the confining effect of the upper soil layers. In the more superficial layers, where confinement is insufficient to counteract soil dilation, displacement tends to be more horizontal. In contrast, at deeper levels, the increased weight of the soil on these layers generates confinement that favours predominantly vertical displacement. Notably, the maximum value of the average angle in Fig.6(c) is 42% lower than that reported by Arshad et al. (2014) in their study on the Cone Penetration Test (CPT).

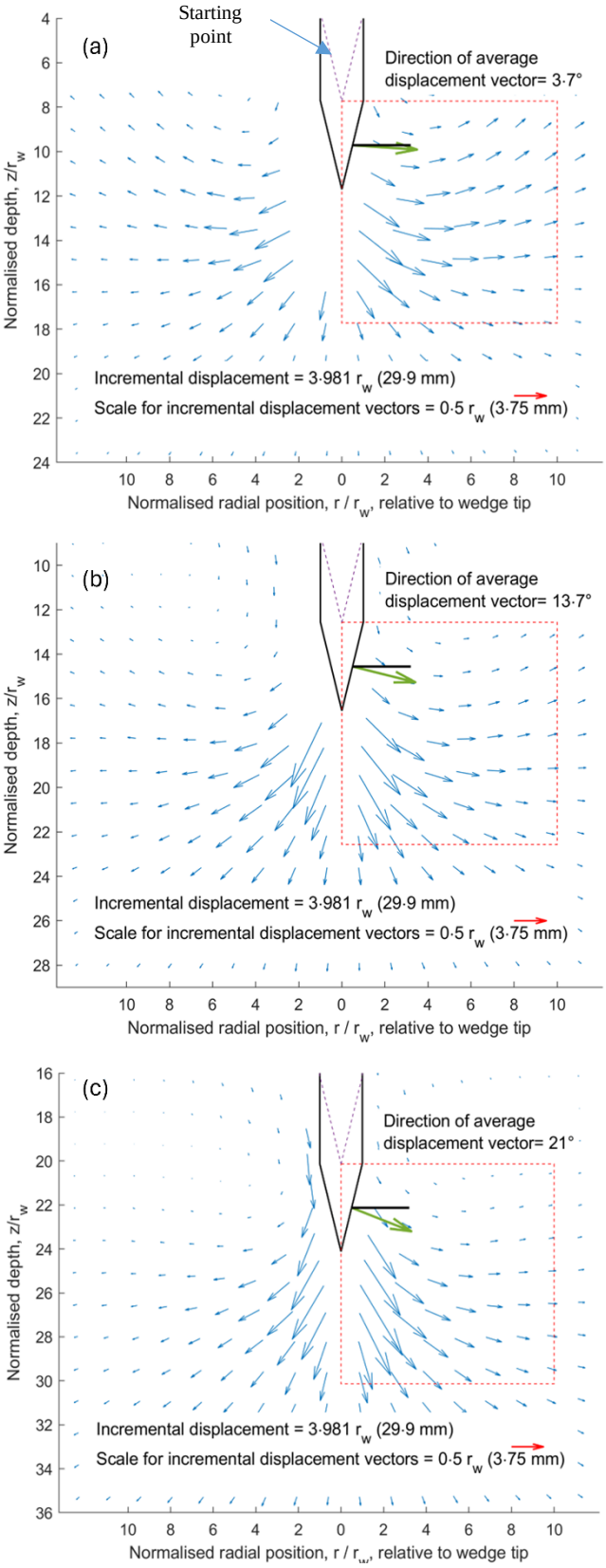

Figure 6. Evolution of slip pattern with penetration: (a) $h/r_w = 7.7$; (b) $h/r_w = 12.5$; (c) $h/r_w = 20$

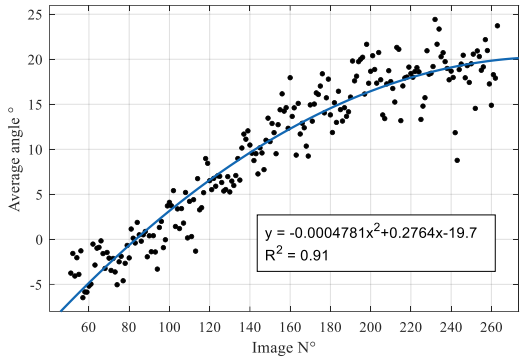

Figure 7. Evolution of average angle with penetration

3.3. Soil strains during wedge penetration

The GeoPIV-RG software has provided a detailed and incremental analysis of shear strain, a critical component for accurately characterizing the mechanical properties of soil. This analysis is indispensable for quantifying the largest shear strain occurring between two consecutive photographic snapshots, corresponding to specific driving intervals. A methodological approach has been applied using a sequence of fifty-one images, the same as used in earlier analyses, to thoroughly monitor the evolution of the incremental strains.

Fig. 8 illustrates a dynamic heat map that captures shear strains during three distinct phases of the penetration process. The analysis of these maps has revealed that the deformations induced by the blade insertion do not exceed 2%. By averaging the shear strain peaks for each interval studied throughout the entire procedure, a maximum average deformation of 1.47% has been determined. This value is in stark contrast to the ranges reported in previous studies related to static cone penetration tests (CPT), such as the one conducted by Melnikov and Boldyrev (2014), where observed deformations ranged from 4% to 100% at the cone's contact interface.

4. Conclusions

In this study, the displacements generated by the insertion of a DMT blade into loose Bío-Bío sand were evaluated using the Particle Image Velocimetry (PIV) technique. It was observed that the disturbance caused by the DMT driving extends approximately 85 mm horizontally and 35 mm vertically at the blade tip. The

analysis of the displacement pattern reveals that as the DMT blade insertion depth increases, the average displacement angle tends towards 21 degrees, which is 42% lower than reported in similar studies using the Cone Penetration Test (CPT). Moreover, the incremental shear strains induced by the DMT blade reached a maximum of 2%, with an average of 1.47%, values notably lower compared to those obtained by the CPT.

Acknowledgements

The first author thanks Engineering Project 2030 (ING222010004) and the Universidad Católica de la Santísima Concepción for funding this research.

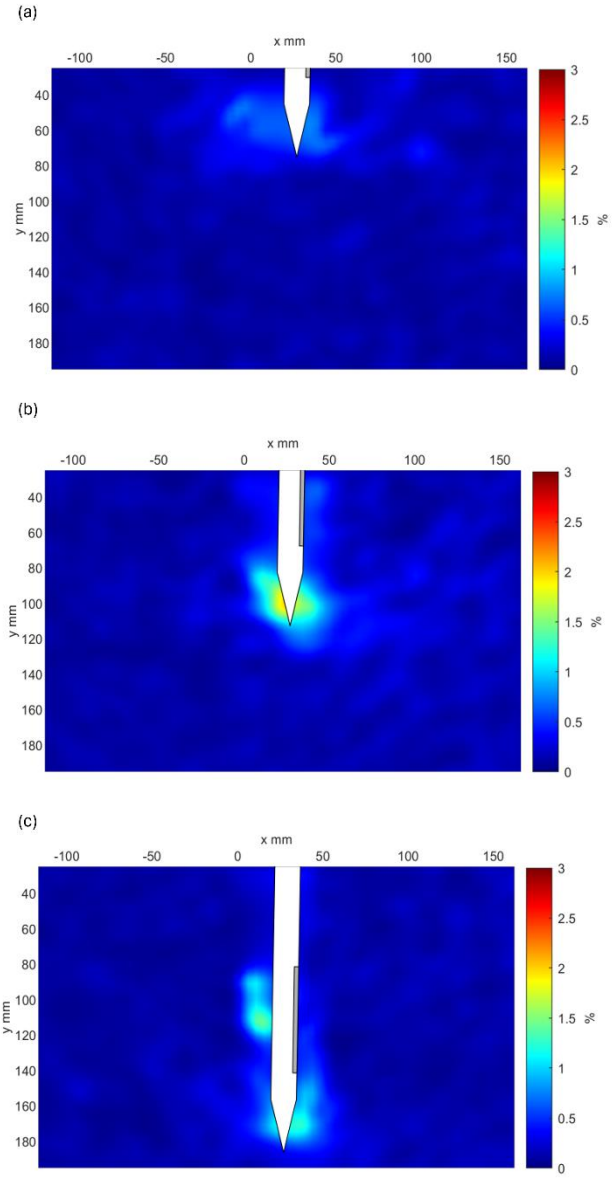

Figure 8. Incremental shear strains for: (a) 76 mm; (b) 112 mm; (c) 185 mm depths

References

Arshad, M.I., F.S. Tehrani, M. Prezzi, and R. Salgado. 2014. 'Experimental Study of Cone Penetration in Silica Sand Using Digital Image Correlation'. *Géotechnique* 64 (7): 551–69. https://doi.org/10.1680/geot.13.P.179.

ASTM D422 (2017). Standard Test Method for Particle-Size Analysis of Soils. West Conshohocken, PA, U.S.A.: American Society for Testing and Materials.

ASTM D4254 (2016). Standard Test Methods for Minimum Index Density and Unit Weight of Soils and Calculation of Relative Density. West Conshohocken, PA, U.S.A.: American Society for Testing and Materials.

ASTM D6635 (2015). Standard Test Method for Performing the Flat Plate Dilatometer. West Conshohocken, PA, U.S.A.: American Society for Testing and Materials.

Bałachowski, L. 2006. 'Penetration Resistance of Lubiatowo Sand in Calibration Chamber Tests'. *Archives of Hydro-Engineering and Environmental Mechanics*, no. Vol. 53, nr 4: 311–29.

Baligh, Mohsen M., and Ronald F. Scott. 1975. 'Quasi-Static Deep Penetration in Clays'. *Journal of the Geotechnical Engineering Division* 101 (11): 1119–33. https://doi.org/10.1061/AJGEB6.0000211.

Bertoli, Dante. 2017. 'Modelado numérico del ensayo dilatómetro de Marchetti'. Memoria de Titulación, Valparaíso, Chile: Universidad Técnica Federico Santa María.

Blaber, J., B. Adair, and A. Antoniou. 2015. 'Ncorr: Open-Source 2D Digital Image Correlation Matlab Software'. *Experimental Mechanics* 55 (6): 1105–22. https://doi.org/10.1007/s11340-015-0009-1.

Butlanska, Joanna, Marcos Arroyo, Sara Amoroso, and Antonio Gens. 2018. 'Marchetti Flat Dilatometer Tests in a Virtual Calibration Chamber'. *Geotechnical Testing Journal* 41 (5): 930–45. https://doi.org/10.1520/GTJ20170370.

Eurocode 7 (1997,2007). Eurocode 7: Geotechnical design - Part 2: Ground Investigation and Testing. European Committee for Standardization. EN 1997-2:2007.

Frost, J D, A Martinez, J Su, and T Xu. 2016. 'Discrete Element Method Modeling Studies of the Interactions between Soils and In-Situ Testing Devices'. In *Fifth International Conference on Geotechnical and Geophysical Site Characterization (ISC'5)*. Gold Coast, Queensland, Australia: International Society for Soil Mechanics and Geotechnical Engineering.

Lee, Moon-Joo, Sung-Kun Choi, Min-Tae Kim, and Woojin Lee. 2011. 'Effect of Stress History on CPT and DMT Results in Sand'. *Engineering Geology* 117 (3–4): 259–65. https://doi.org/10.1016/j.enggeo.2010.11.005.

Luo, S., and C. Xu. 2012. 'Numeric Modeling of the Flat Dilatometer Test', April, 269–76. https://doi.org/10.1061/40861(193)35.

Marchetti, Silvano. 1980. 'In Situ Tests by Flat Dilatometer'. *Journal of the Geotechnical Engineering Division* 106 (3): 299–321. https://doi.org/10.1061/AJGEB6.0000934.

Melnikov, A., and G. Boldyrev. 2014. 'Experimental Study of Sand Deformations during a CPT'. In *3rd International Symposium on Cone Penetration Testing*. Las Vegas, Nevada, USA.

Mo, Pin-Qiang, Alec Marshall, and H Yu. 2012. 'Centrifuge Modelling of CPT in Layered Soils'. In *Geotechnical and Geophysical Site Characterization 4, ISC 4*, 219–25. Porto de Galinhas, Pernambuco, Brazil.

Nazhat, Yahya, and David Airey. 2011. 'Validation of High Speed Photography and PIV in Large Strain Measurements of Granular Materials'. In *9th International Symposium on Particle Image Velocimetry - PIV'11*. Kobe, Japan.

Ngo, Tan-Phong, and Thuy-Chung Kieu-Le. 2021. 'Application of Particle Image Velocimetry (PIV) to Measure the Displacement of Sandy Soil in Laboratory'. *Vietnam Journal of Science, Technology and Engineering* 63 (3): 70–77. https://doi.org/10.31276/VJSTE.63(3).70-77.

Pan, Bing, Kemao Qian, Huimin Xie, and Anand Asundi. 2009. 'Two-Dimensional Digital Image Correlation for in-Plane Displacement and Strain Measurement: A Review'.

Measurement Science and Technology 20 (6): 062001. https://doi.org/10.1088/0957-0233/20/6/062001.

Schreier, Hubert W., and Michael A. Sutton. 2002. 'Systematic Errors in Digital Image Correlation Due to Undermatched Subset Shape Functions'. *Experimental Mechanics* 42 (3): 303–10. https://doi.org/10.1007/BF02410987.

Stanier, S. A., and D. J. White. 2013. 'Improved Image-Based Deformation Measurement in the Centrifuge Environment'. *Geotechnical Testing Journal* 36 (6): 915–28. https://doi.org/10.1520/GTJ20130044.

Stanier, S.A., J. Blaber, W.A. Take, and D.J. White. 2016. 'Improved Image-Based Deformation Measurement for Geotechnical Applications'. *Canadian Geotechnical Journal* 53 (5): 727–39. https://doi.org/10.1139/cgj-2015-0253.

White, D. J., and M. D. Bolton. 2002. 'Soil Deformation around a Displacement Pile in Sand'. In *Physical Modelling in Geotechnics*, by P. Guo, R. Phillips, and R. Popescu, 1st ed., 649–54. London: Routledge. https://doi.org/10.1201/9780203743362-118.

White, David, WA Take, and Malcolm Bolton. 2003. 'Soil Deformation Measurement Using Particle Image Velocimetry (PIV) and Photogrammetry'. *Geotechnique* 53 (January): 619–31. https://doi.org/10.1680/geot.53.7.619.37383.

Xu, Tianlong, and J David Frost. 2015. 'DEM Modeling of Insertion and Expansion during Flat Dilatometer Testing'. In *Third International Conference on the Flat Dilatometer*, 439–46. Rome, Italy: International Society of Soil Mechanics and Geotechnical Engineering, London, United Kingdom.